

Possible bump structure of cosmic ray electrons unveiled by AMS-02 data

PEI-PEI ZHANG,¹ BING-QIANG QIAO,² WEI LIU,² SHU-WANG CUI,¹ QIANG YUAN,^{3,4,5} AND YI-QING GUO^{2,6}

¹ *Hebei Normal University, Shijiazhuang 050024, Hebei, China*

² *Key Laboratory of Particle Astrophysics, Institute of High Energy Physics, Chinese Academy of Sciences, Beijing 100049, China*

³ *Key Laboratory of Dark Matter and Space Astronomy, Purple Mountain Observatory, Chinese Academy of Sciences, Nanjing 210008, China*

⁴ *School of Astronomy and Space Science, University of Science and Technology of China, Hefei 230026, China*

⁵ *Center for High Energy Physics, Peking University, Beijing 100871, China*

⁶ *University of Chinese Academy of Sciences, Beijing 100049, China*

ABSTRACT

The precise measurement of the positron spectrum by AMS-02 reveals a sharp dropoff above ~ 284 GeV. However, the AMS-02 electron spectrum shows a power-law from ~ 40 GeV to ~ 1 TeV without significant features. We propose that the difference of spectral features between electrons and positrons indicates the existence of a nearby source component of primary electrons. Taking into account the observational results of the positron excess, the spectral softenings of cosmic ray protons and helium nuclei, and the energy-dependences of the large-scale anisotropies of cosmic rays, we suggest that the scenario of supernova remnant origin of cosmic rays with non-negligible contribution from a nearby source can successfully account for most of the observations of cosmic rays below PeV energies. The Geminga pulsar and its past supernova remnant might be a proper candidate of the nearby source.

1. INTRODUCTION

The uncovered features in the cosmic-rays (CRs) electron/positron energy spectra by the precise observations help us better understand their origin, acceleration and propagation in Galaxy. The increasing positron fraction above 10 GeV (Adriani et al. 2009; Accardo et al. 2014; Aguilar et al. 2019b) had called a lot of attention. It indicates an additional primary positron component, which is incompatible with the conventional propagation picture. A number of alternatives have been proposed, which can be either astrophysical, such as local pulsars and the hadronic interactions inside SNRs, or even more exotic dark matter self-annihilation or decay (He 2009; Fan et al. 2010; Serpico 2012; Cirelli 2012; Bi et al. 2013).

The hardening of electron spectrum above ~ 50 GeV has also been confirmed by observations of DAMPE and AMS-02 experiments (DAMPE Collaboration et al. 2017; Aguilar et al. 2019a). One possibility is that there are two different types of Galactic lepton sources (Aguilar et al. 2019a). The Klein Nishina effect of the inverse Compton scattering may also have some effect on regulating the electron spectrum (Stawarz et al. 2010; Evoli et al. 2020; Fang et al. 2020). In a recent work,

we demonstrated that the hardening may originate from the spatial-dependent propagation process (Tian et al. 2020).

Moreover, the drop-off around 1 TeV in the all-electron spectrum was first reported by HESS collaboration (Aharonian et al. 2009, 2008; Kerszberg 2017). Afterwards this breakoff was validated by MAGIC (Borla Tridon 2011), VERITAS (Staszak et al. 2015) experiments. DAMPE experiment performed the first direct measurement to this feature (DAMPE Collaboration et al. 2017). It is argued that the break-off results from the radiation cooling of electrons surrounding SNRs (Vannoni et al. 2009) or the threshold interaction during the transport of cosmic-ray electrons (Hu et al. 2009; Wang et al. 2010; Jin et al. 2016).

In the latest publications, AMS-02 collaboration has measured cosmic-ray electrons and positrons (CREs) up to 1.4 TeV and 1 TeV respectively (Aguilar et al. 2019a,b). Apart from confirming the earlier findings, a sharp dropoff of positron flux above ~ 284 GeV is reported for the first time. But the power-law behavior in the electron spectrum extends to at least 1.9 TeV. It is slightly different from the measurements of HESS (Aharonian et al. 2009, 2008; Kerszberg 2017), DAMPE (DAMPE Collaboration et al. 2017) and CALET (Adriani et al. 2018), in which a spectral break at about 0.9 TeV has been found. Nevertheless the reported break

energy of positron is still visibly lower than that of electron.

In this work, we demonstrate that the difference of spectral cutoff of electron and positron strongly indicates the existence of a nearby source component of primary electrons. Besides the secondary production of positrons during CR's spatially dependent propagation (SDP) in Galaxy, we also consider a local pulsar, which contributes the primary positrons to account for the positron excess. Our calculations show that even taking both contributions into account, the all-electron spectrum still could not be described above ~ 500 GeV. There is an additional electron component between 500 GeV and 2 TeV, which shows a bump-like structure. We find under the appropriate parameters, this feature could be well described by Geminga SNR. It's worth noting that similar origins are predicted in (Yuan & Bi 2013; Evoli et al. 2012; Cholis & Hooper 2013; Li et al. 2015; Fornieri et al. 2020).

In our previous work, we propose a simple picture, based on the SDP scenario, to account for the observational features of GCR energy spectra and anisotropies. The spectral bumps of GCR protons and helium between 200 GV and tens of TV, reported by CREAM (Yoon et al. 2017), NUCLEON (Atkin et al. 2017), DAMPE (An et al. 2019), can be well described by a background component and a local source component of GCRs. The sum of the streamings of the background and local source components, can naturally explain the spectral evolutions. The low-energy (≤ 100 TeV) anisotropies are dominated by the local source, while the high-energy anisotropies are due to the background. The transition of the low-energy and high-energy components occur at about 100 TeV, forming a dip in the amplitude and a flip of the phase from nearly anti-Galactic center direction to the Galactic center direction. We also point that Geminga SNR could be such local source. Meanwhile Geminga pulsar could be the source of positron excess. Then coupled with difference of spectral cutoff of electron and positron, all of the observational features below tens of PeV could be accounted for in our unified picture.

The rest paper is organized in the following way. In Sec.2, the spatial-dependent propagation and corresponding model are introduced briefly. Sec.3 presents the calculated results and Sec.4 is reserved for the conclusion.

2. MODEL DESCRIPTION

2.1. Spatial-dependent propagation

The spatial-dependent propagation (SDP) of CRs has received a lot of attention in recent years. It was first

introduced as a Two Halo model (THM) (Tomassetti 2012) to explain the spectral hardening of both proton and helium above 200 GeV (Adriani et al. 2011). Afterwards, it is further applied to secondary and heavier components (Tomassetti 2015; Feng et al. 2016; Guo et al. 2016; Liu et al. 2018; Tian et al. 2020; Yuan et al. 2020), diffuse gamma-ray distribution (Guo & Yuan 2018) and large-scale anisotropy (Liu et al. 2019; Qiao et al. 2019). For a comprehensive introduction, one can refer to Guo et al. (2016) and Liu et al. (2018).

In the SDP model, the whole diffusive halo is divided into two parts. The Galactic disk and its surrounding area are called the inner halo (IH) region, in which the diffusion coefficient is spatial dependent and relevant to the radial distribution of background CR sources. The extensive diffusive region outside the IH is named as the outer halo (OH) region, where the diffusion is regarded as only rigidity dependent. The spatial-dependent diffusion coefficient D_{xx} is thus parameterized as:

$$D_{xx}(r, z, \mathcal{R}) = D_0 F(r, z) \beta^\eta \left(\frac{\mathcal{R}}{\mathcal{R}_0} \right)^{\delta(r, z)}. \quad (1)$$

For the parameterization of $F(r, z)$ and $\delta(r, z)$, one can refer to Tian et al. (2020). The size of IH is represented by its half thickness ξz_h , whereas the OH region's is $(1 - \xi) z_h$.

In this work, we adopt the common diffusion-reacceleration (DR) model, with the diffusive-reacceleration coefficient D_{pp} coupled to D_{xx} by $D_{pp} D_{xx} = \frac{4p^2 v_A^2}{3\delta(4 - \delta^2)(4 - \delta)}$, in which v_A is the so-called Alfvén velocity (Seo & Ptuskin 1994). The numerical package DRAGON is used to solve the SDP equation to obtain the distribution of CREs. During the propagation, the energetic CREs still suffer from the energy loss from synchrotron radiation and inverse Compton scattering (Strong & Moskalenko 1998; Moskalenko & Strong 1998). A full-relativistic treatment of the inverse-Compton losses (Delahaye et al. 2010) has been implemented in the DRAGON package (Evoli et al. 2017). Less than tens of GeV, the CR fluxes are impacted by the solar modulation. The well-known force-field approximation (Gleeson & Axford 1968; Perko 1987) is applied to describe such an effect, with a modulation potential ϕ adjusted to fit the low energy data.

2.2. Supernova remnants

The supernova remnants (SNRs) are regarded as the most likely sites for the acceleration of cosmic rays (CRs) by default, in which the charge particles are accelerated to a power-law distribution through the diffusive shock acceleration. The distribution of SNRs are ap-

proximated as an axisymmetric, which is usually parameterized as

$$f(r, z) = \left(\frac{r}{r_\odot}\right)^\alpha \exp\left[-\frac{\beta(r-r_\odot)}{r_\odot}\right] \exp\left(-\frac{|z|}{z_s}\right), \quad (2)$$

where $r_\odot \equiv 8.5$ kpc represents the solar distance to the Galactic center. The parameters α and β are taken as 1.09 and 3.87 respectively in this work (Green 2015). Perpendicular to the Galactic plane, the density of CR sources descends exponentially, with a mean value $z_s = 100$ pc. The axisymmetric approximation is plausible as the diffusion length of CR nuclei is usually much longer than the characteristic spacing between the neighbouring spiral arms. However, subject to the energy loss from synchrotron radiation and inverse Compton scattering, the transport distance of the energetic electrons is much shorter so that the above approximation may no longer hold. Thus the inclusion of a more realistic description of the source distribution is expected to have striking impact on the observed spectrum of high-energy electrons.

As is well-known, our Milky Way is a spiral galaxy. In this work, the spiral distribution of SNRs follows the model established by Faucher-Giguère & Kaspi (2006). The Galaxy consists of four major arms, with the locus of the i -th arm centroid expressed as a logarithmic curve: $\theta(r) = k^i \ln(r/r_0^i) + \theta_0^i$, where r is the distance to the Galactic center. For the values of k^i , r_0^i and θ_0^i for each arm, one can refer to Tian et al. (2020). Along each spiral arm, there is a spread in the normal direction which follows a Gaussian distribution, i.e.

$$f_i = \frac{1}{\sqrt{2\pi}\sigma_i} \exp\left[-\frac{(r-r_i)^2}{2\sigma_i^2}\right], \quad i \in [1, 2, 3, 4], \quad (3)$$

where r_i is the inverse function of the i -th spiral arm's locus and σ_i is equal to $0.07r_i$. The number density of SNRs at different radii still conforms with the radial distribution in the axisymmetric case, i.e. Eq (2). The injection spectrum of CRE are assumed to have a broken power-law, i.e.

$$q^{e^-}(\mathcal{R}) = q_0^{e^-} \begin{cases} \left(\frac{\mathcal{R}}{\mathcal{R}_{\text{br}}^{e^-}}\right)^{\nu_1^{e^-}}, & \mathcal{R} \leq \mathcal{R}_{\text{br}1}^{e^-} \\ \left(\frac{\mathcal{R}}{\mathcal{R}_{\text{br}}^{e^-}}\right)^{\nu_2^{e^-}}, & \mathcal{R}_{\text{br}1}^{e^-} < \mathcal{R} < \mathcal{R}_{\text{br}2}^{e^-} \\ \left(\frac{\mathcal{R}}{\mathcal{R}_{\text{br}}^{e^-}}\right)^{\nu_3^{e^-}}, & \mathcal{R} > \mathcal{R}_{\text{br}2}^{e^-} \end{cases} \quad (4)$$

where q_0 , ν and R_{br} are the normalization, spectral index, and broken rigidity respectively.

2.3. Local Pulsar

At \sim TeV energies, the CR electrons and positrons originate from sources within 1 kpc around the solar system. In this small region, the continuity hypothesis is no longer valid. Studies show that the discrete effect of nearby CR sources could induce large statistical fluctuations (Mertsch 2011; Bernard et al. 2012), especially at high energies. The contribution of nearby sources to CREs has been studied in the past works (see Serpico (2012); Di Mauro et al. (2014); Liu et al. (2017); Abeysekara et al. (2017); Fang et al. (2018) and references therein). In this work, we assume a nearby pulsar to account for the positron excess above ~ 20 GeV. The propagation of CREs injected instantaneously from a point source is described by a time-dependent propagation equation and the corresponding solution $G(\mathbf{r}, t, E)$ can be found in Kobayashi et al. (2004). The energy dependence is taken as a single power-law distribution, namely

$$Q(E, t) = Q_0(t) \left(\frac{\mathcal{R}}{1 \text{ GV}}\right)^{-\gamma} \exp\left[-\frac{\mathcal{R}}{\mathcal{R}_c^{e^\pm}}\right], \quad (5)$$

with $\mathcal{R}_c^{e^\pm}$ the cutoff rigidity. For the local pulsar, a continuous injection process of electron-positron pairs is considered. The injection rate is time-dependent, decays as

$$Q_0(t) = \frac{q_0}{[1 + (t - t_i)/\tau_0]^2}, \quad (6)$$

where t_i and τ_0 are the initial injection time and characteristic duration (Kawanaka et al. 2010; Yin et al. 2013). The observed spectrum from local pulsar is thus a convolution of Green function and time-dependent injection rate $Q_0(t)$ (Kawanaka et al. 2010; Kisaka & Kawanaka 2012), i.e.

$$\varphi(\mathbf{r}, E, t) = \int_{t_i}^t G(\mathbf{r} - \mathbf{r}', t - t', E) Q_0(t') dt'. \quad (7)$$

3. RESULTS

The propagation parameters used in this work refer to Tian et al. (2020), which well fit the recent observations of proton, helium and B/C ratio. The corresponding injected spectra of proton and helium are applied to calculate the yields of secondary electrons and positrons during the transport, with the production cross section taken from the Fluka package (Mazziotta et al. 2016). The local pulsar is assumed to be 0.25 kpc away from the solar system and 2×10^5 years old.

Figure 1 illustrates the calculated spectra of positrons (top), electrons (middle) and all-electrons (bottom). For both electrons and positrons, the measurements by the AMS-02 experiment are taken. As for all-electron spectra, the latest observation of HESS is also

included as blue data points. The blue and yellow solid lines are the primary electrons from SNRs and secondary electrons/positrons generated during the propagation respectively. The green solid lines are the electrons/positrons generated by the local pulsar.

First of all, we attempt to account for the positron excess, which is shown in the left of Figure 1. As can be seen that due to the SDP, the propagated background positron and electron spectra flatten above tens of GeV, compared with the conventional propagation model. This is similar to the spectral hardening of cosmic-ray nuclei during SDP. But unlike the CR nuclei, the energy loss of electrons shifts that excess to the lower energy, i.e. about tens of GeV. This is consistent with the hardening of electrons uncovered by the recent experiments. Meanwhile due to the FLUKA generation cross section as well as the SDP + spiral scenario, the background secondary positron flux also enhances overall greatly so that the positron spectrum above 10 GeV could be well accounted for. These features have been extensively discussed in the previous work (Tian et al. 2020).

The calculations show that to describe the positron break at ~ 284 GeV, as shown in the top left of Figure 1, the cutoff rigidity R_c in the injection spectrum of the local pulsar is 800 GV. However we notice that when adopting this value, both electron and all-electron spectra are inadequate to explain above ~ 500 GeV. This is particularly evident in the all-electron spectrum when we allow for the HESS data above 1 TeV. The calculated all-electron flux is far less than the measurements between 500 GeV and 2 TeV.

We further change the cutoff rigidity R_c to fit the all-electron spectrum and study its influence of the TeV break on the positron spectrum, as demonstrated in the right of Figure 1. In this case, R_c is 2300 GV in order to fit the all-electron spectrum. But the positron flux continue rising above 200 GeV until ~ 600 GeV then drop off. Its flux significantly exceeds the latest AMS-02 measurements above ~ 300 GeV. This excess results from the higher energy cutoff of the positrons. Therefore it is obvious that if the drop-off of positron flux measured by the AMS-02 experiment is correct, inevitably there are extra electrons.

It should be emphasized that this excess also holds for other measurements, e.g. DAMPE. Compared with AMS-02, the DAMPE experiment could observe CREs beyond TeV energies, from tens of GeV to 5 TeV, well covering the energy range of our concern. But the measured all-electron flux is overall higher than that of AMS-02 when the energies exceed 70 GeV. Moreover, it has no measurements of electrons and positrons be-

cause it is incapable of separating positrons from electrons. Nevertheless, for the background component, the electron flux far exceeds the positron flux, therefore the background flux could be approximated as the electron contribution. The parameters of electron flux fitting DAMPE experiment are listed in 1. Since the measured all-electron spectrum by dampe is harder than ams-02, the background electron flux is harder, with power index is 2.55 less than 1100 GeV and 3.0 above that energy. It can be found that to explain the whole energy range of DAMPE experiment, the high energy cutoff of local pulsar have to be 2300, i.e. model B, as shown in the right of figure 2. If the cutoff rigidity of model A are adopted, the similar absence also appears at around TeV energies, see the left of figure 2.

The feature of excess in the all-electron spectrum are further studied. After subtracting the theoretical model from the experimental data points, an additional bump of electrons appears, which is shown as circles in Figure 3. The red circles are the residuals of AMS-02 minus model, whereas the blue circles are the residuals of HESS minus model. We can see both residual are consistent. The residual electrons for DAMPE measurement are shown in the right of Figure 3.

One of the possible origins for this excess is a local SNR. In our unified picture (Liu et al. 2019; Qiao et al. 2019), we apply a local source, i.e. Geminga SNR, to account for both spectral hardening of CR nuclei and large-scale anisotropy. Meanwhile the Geminga pulsar is believed to be source of the positron excess. Here we assume this source likewise contribute the extra electrons. To describe this electron bump, the injection spectrum of this local SNR is assumed to have a single power-law, i.e.

$$Q(E, t) = q_l \left(\frac{\mathcal{R}}{1 \text{ GV}} \right)^{-\beta} \exp \left[-\frac{\mathcal{R}}{\mathcal{R}_c} \right], \quad (8)$$

The result is shown in Figure 3. As can be seen that both bumps of HESS and DAMPE are consistent and they can be well described by a time dependent propagation of local electrons. The injected parameters used to fit HESS are also hold for DAMPE, which are listed in table 1.

4. CONCLUSION

The precise measurements of cosmic-rays enable us to better reveal their origins. Recently, AMS-02 collaboration have upgraded their measurements of cosmic-ray electrons and positrons. Compared with the previous observations, a new positron break-off above ~ 284 GeV has been found. This is different from the electron spectrum, whose power-law spectrum extends to the higher

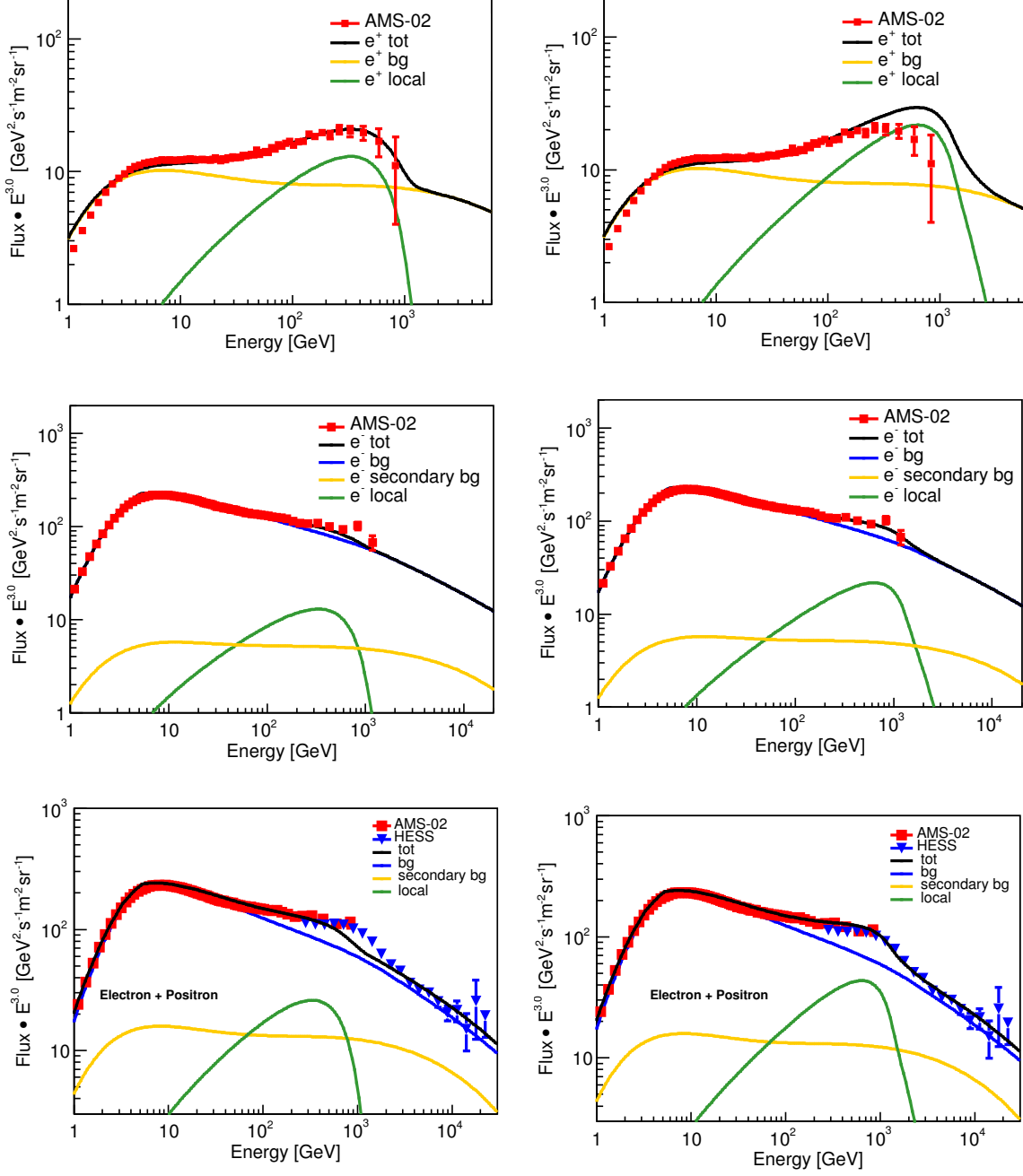


Fig. 1. Calculated spectra of positrons(top), electrons(middle) and all-electrons(bottom). The red and blue data points are measured by AMS-02 and HESS experiments. In the left figures, \mathcal{R}_c of the injection spectrum of local pulsar is 800 GV, while in the right figures, \mathcal{R}_c is 2300 GV. All of the propagated and injection parameters are listed in table 1.

energy and has a break at about TeV energies. In this work, we study the high energy cutoff of electron and positron spectra based on the SDP model. A conventional SNR background plus local pulsar model is applied. We find there is a tension in the high energy cutoff between the positron and all-electron spectra in this simple scenario. Compared with all-electron spectrum, which requires the cutoff rigidity of local pulsar

is 2300 GV, to well fit positron dropoff, the high energy cutoff of the local pulsar is just 800 GV. Therefore if the observed cutoff of positron flux is correct, there are extra electrons from 500 GeV to 2 TeV which are not accounted for. This excess of electrons has not been claimed as far as we know.

After subtracting the calculated electron and positron fluxes from the measured all-electron spectrum, the ex-

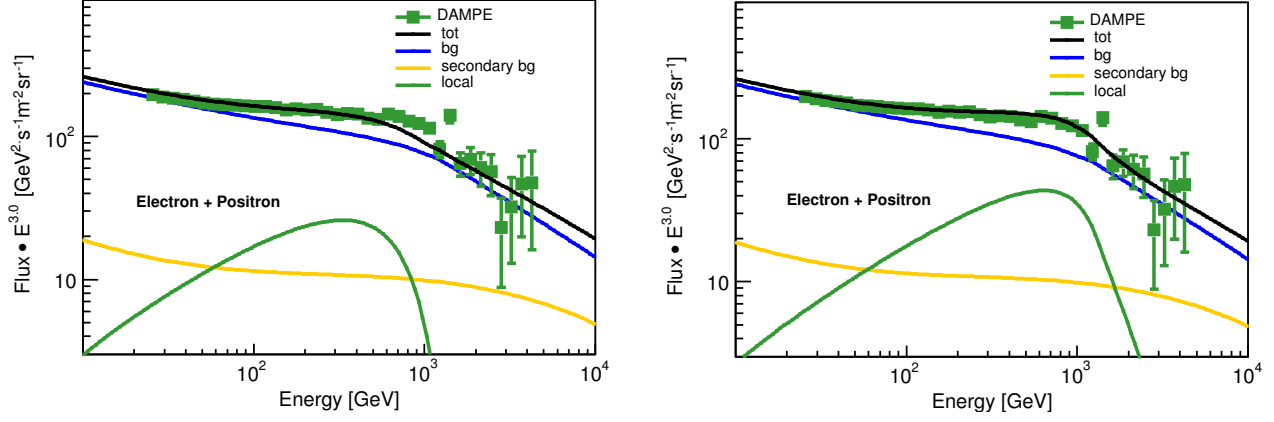


Fig. 2. The same calculation for DAMPE.

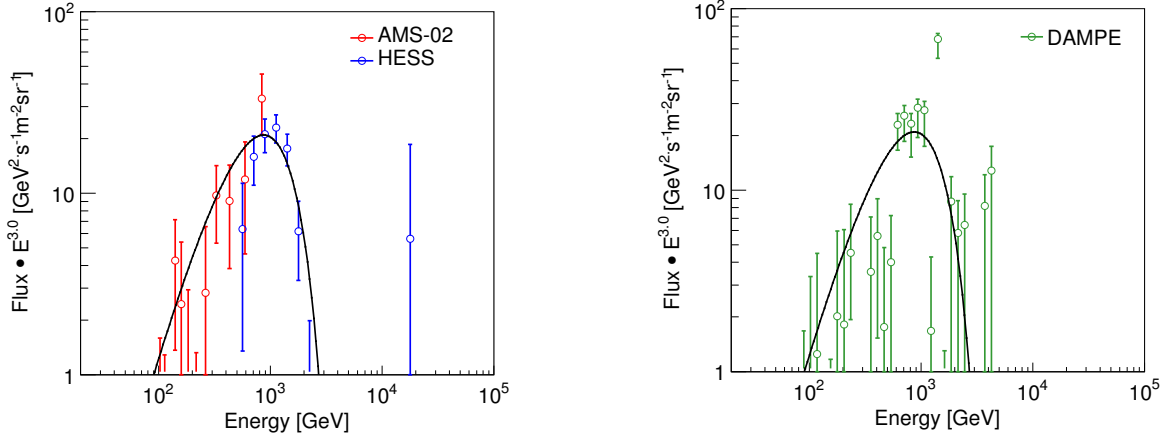


Fig. 3. Calculation of time-dependent propagation of electrons from a Geminga SNR to explain the electron excess above 500 GeV.

Tab. 1. injected parameters of electrons and positrons from background SNRs and local pulsar.

background	A [$\text{m}^{-2}\text{sr}^{-1}\text{s}^{-1}\text{GeV}^{-1}$] [†]	ν_1	\mathcal{R}_{br1} [GV]	ν_2	\mathcal{R}_{br2} [GV]	ν_3
e^- for HESS fitting	3.01×10^{-1}	1.14	5.1	2.69	1500	2.8
e^- for DAMPE fitting	2.4×10^{-1}			2.55	1100	3.0
local pulsar	r [kpc]	t_0 [yrs]	q_0 [GeV^{-1}]	γ	τ_0 [yrs]	$\mathcal{R}_c^{\text{e}\pm}$ [GV]
A	0.25	2×10^5	9.85×10^{49}	2.25	10^4	800
B	0.25	2×10^5	1.15×10^{50}	2.25	5×10^4	2300
local SNR	r [kpc]	t [yrs]	q_l [GeV^{-1}]	β	\mathcal{R}_c [GV]	
	0.34	3.4×10^5	2.25×10^{51}	1.9	550	

[†]The normalization is set at kinetic energy $E_k = 100$ GeV for proton and $E_k = 10$ GeV for electron.

cessive electrons has a bump-like structure. And we show this excess is common whatever AMS-02, HESS or DAMPE measurements. This feature indicates an origin of local sources. One of probable source is

Geminga SNR. This source has been used to account for both spectral hardening of CR nuclei and large-scale anisotropy. Meanwhile the Geminga pulsar is widely believed to be source of the positron excess. We find that

the extra component could be decently explained by the Geminga SNR. Therefore the observational features of Galactic cosmic rays could be accounted for in our unified picture with SNR background plus a local source, even this excess of electrons. At present, the measurements of positrons above 200 GeV are still inaccurate,

with quite large errors. We expect the coming precise measurements could testify our speculation.

ACKNOWLEDGEMENTS

This work is supported by the National Key R&D Program of China grant No. 2018YFA0404203, the National Natural Science Foundation of China (Nos. 11635011, U1831129, 111722328, 11851305, U1738205, 11875264, U2031110).

REFERENCES

- Abeyssekara, A. U., Albert, A., Alfaro, R., et al. 2017, *Science*, 358, 911
- Accardo, L., Aguilar, M., Aisa, D., et al. 2014, *Physical Review Letters*, 113, 121101
- Adriani, O., Barbarino, G. C., Bazilevskaya, G. A., et al. 2009, *Nature*, 458, 607
- . 2011, *Science*, 332, 69
- Adriani, O., Akaike, Y., Asano, K., et al. 2018, *Phys. Rev. Lett.*, 120, 261102
- Aguilar, M., Ali Cavasonza, L., Alpat, B., et al. 2019a, *Phys. Rev. Lett.*, 122, 101101
- Aguilar, M., Ali Cavasonza, L., Ambrosi, G., et al. 2019b, *Phys. Rev. Lett.*, 122, 041102
- Aharonian, F., Akhperjanian, A. G., Barres de Almeida, U., et al. 2008, *Physical Review Letters*, 101, 261104
- Aharonian, F., Akhperjanian, A. G., Anton, G., et al. 2009, *A&A*, 508, 561
- An, Q., Asfandiyarov, R., Azzarello, P., et al. 2019, *Science Advances*, 5, eaax3793
- Atkin, E., Bulatov, V., Dorokhov, V., et al. 2017, *J. Cosmology Astropart. Phys.*, 7, 020
- Bernard, G., Delahaye, T., Salati, P., & Taillet, R. 2012, *A&A*, 544, A92
- Bi, X.-J., Yin, P.-F., & Yuan, Q. 2013, *Frontiers of Physics*, 8, 794
- Borla Tridon, D. 2011, *International Cosmic Ray Conference*, 6, 47
- Cholis, I., & Hooper, D. 2013, *Phys. Rev. D*, 88, 023013
- Cirelli, M. 2012, *Pramana*, 79, 1021
- DAMPE Collaboration, Ambrosi, G., An, Q., et al. 2017, *Nature*, 552, 63
- Delahaye, T., Lavalle, J., Lineros, R., Donato, F., & Fornengo, N. 2010, *A&A*, 524, A51
- Di Mauro, M., Donato, F., Fornengo, N., Lineros, R., & Vittino, A. 2014, *J. Cosmology Astropart. Phys.*, 4, 6
- Evoli, C., Blasi, P., Amato, E., & Aloisio, R. 2020, *Phys. Rev. Lett.*, 125, 051101
- Evoli, C., Gaggero, D., Grasso, D., & Maccione, L. 2012, *Physical Review Letters*, 108, 211102
- Evoli, C., Gaggero, D., Vittino, A., et al. 2017, *J. Cosmology Astropart. Phys.*, 2, 015
- Fan, Y.-Z., Zhang, B., & Chang, J. 2010, *International Journal of Modern Physics D*, 19, 2011
- Fang, K., Bi, X.-J., Lin, S.-J., & Yuan, Q. 2020, arXiv e-prints, arXiv:2007.15601
- Fang, K., Bi, X.-J., & Yin, P.-F. 2018, *ApJ*, 854, 57
- Faucher-Giguère, C.-A., & Kaspi, V. M. 2006, *ApJ*, 643, 332
- Feng, J., Tomassetti, N., & Oliva, A. 2016, *Phys. Rev. D*, 94, 123007
- Fornieri, O., Gaggero, D., Guberman, D., Brahimi, L., & Marcowith, A. 2020, arXiv e-prints, arXiv:2007.15321
- Gleeson, L. J., & Axford, W. I. 1968, *ApJ*, 154, 1011
- Green, D. A. 2015, *MNRAS*, 454, 1517
- Guo, Y.-Q., Tian, Z., & Jin, C. 2016, *ApJ*, 819, 54
- Guo, Y.-Q., & Yuan, Q. 2018, *Phys. Rev. D*, 97, 063008
- He, X.-G. 2009, *Modern Physics Letters A*, 24, 2139
- Hu, H.-B., Yuan, Q., Wang, B., et al. 2009, *ApJ*, 700, L170
- Jin, C., Liu, W., Hu, H.-B., & Guo, Y.-Q. 2016, arXiv e-prints, arXiv:1611.08384
- Kawanaka, N., Ioka, K., & Nojiri, M. M. 2010, *ApJ*, 710, 958
- Kerszberg, D. f. 2017
- Kisaka, S., & Kawanaka, N. 2012, *MNRAS*, 421, 3543
- Kobayashi, T., Komori, Y., Yoshida, K., & Nishimura, J. 2004, *ApJ*, 601, 340
- Li, X., Shen, Z.-Q., Lu, B.-Q., et al. 2015, *Physics Letters B*, 749, 267
- Liu, W., Bi, X.-J., Lin, S.-J., Wang, B.-B., & Yin, P.-F. 2017, *Phys. Rev. D*, 96, 023006
- Liu, W., Guo, Y.-Q., & Yuan, Q. 2019, *J. Cosmology Astropart. Phys.*, 2019, 010
- Liu, W., Yao, Y.-h., & Guo, Y.-Q. 2018, *ApJ*, 869, 176
- Mazzotta, M. N., Cerutti, F., Ferrari, A., et al. 2016, *Astroparticle Physics*, 81, 21
- Mertsch, P. 2011, *J. Cosmology Astropart. Phys.*, 2, 31

- Moskalenko, I. V., & Strong, A. W. 1998, *ApJ*, 493, 694
- Perko, J. S. 1987, *A&A*, 184, 119
- Qiao, B.-Q., Liu, W., Guo, Y.-Q., & Yuan, Q. 2019, *J. Cosmology Astropart. Phys.*, 2019, 007
- Seo, E. S., & Ptuskin, V. S. 1994, *ApJ*, 431, 705
- Serpico, P. D. 2012, *Astroparticle Physics*, 39, 2
- Staszak, D., Abeysekara, A. U., Archambault, S., et al. 2015, *ArXiv e-prints*, arXiv:1510.01269
- Stawarz, L., Petrosian, V., & Blandford, R. D. 2010, *ApJ*, 710, 236
- Strong, A. W., & Moskalenko, I. V. 1998, *ApJ*, 509, 212
- Tian, Z., Liu, W., Yang, B., et al. 2020, *Chinese Physics C*, 44, 085102
- Tomassetti, N. 2012, *ApJ*, 752, L13
- . 2015, *Phys. Rev. D*, 92, 081301
- Vannoni, G., Gabici, S., & Aharonian, F. A. 2009, *A&A*, 497, 17
- Wang, B., Yuan, Q., Fan, C., et al. 2010, *Science China Physics, Mechanics, and Astronomy*, 53, 842
- Yin, P.-F., Yu, Z.-H., Yuan, Q., & Bi, X.-J. 2013, *Phys. Rev. D*, 88, 023001
- Yoon, Y. S., Anderson, T., Barrau, A., et al. 2017, *ApJ*, 839, 5
- Yuan, Q., & Bi, X.-J. 2013, *Physics Letters B*, 727, 1
- Yuan, Q., Qiao, B.-Q., Guo, Y.-Q., Fan, Y.-Z., & Bi, X.-J. 2020, *arXiv e-prints*, arXiv:2007.01768